Transient Modeling of Large Scale Integrated Refrigeration and Storage Systems

A M Swanger[1]

[1]NASA Kennedy Space Center, Cryogenics Test Laboratory, Kennedy Space Center, FL 32899 USA

Email: adam.m.swanger@nasa.gov

Abstract. Recently, next generation techniques and designs were demonstrated using Integrated Refrigeration and Storage (IRAS) for large scale storage of liquid hydrogen at NASA Kennedy Space Center (KSC) in Florida. Zero boil-off, densification, and in-situ liquefaction of hydrogen were achieved at various fill levels inside a custom-built 125,000 liter, horizontal-cylindrical IRAS tank, validating the applicability of the concept for large scale cryo-fluid storage architectures. This paper will discuss a number of transient physics models developed to predict the bulk behavior of large IRAS systems, and the comparison of those models to data gathered during the KSC test campaign. In an attempt to extend their usefulness to future IRAS designs, these models were agnostic with respect to stored fluid, tank size and geometry. Behavior during densification testing was examined at three fill levels, and ultimately the depressurization and bulk temperature trends of the KSC tests were predicted with good accuracy.

1. Introduction

Beginning in 2015, research engineers at NASA Kennedy Space Center (KSC) brought a next generation, large scale liquid hydrogen (LH_2) system online to demonstrate advanced storage and transfer concepts and operations. This system, deemed the Ground Operations Demonstration Unit for Liquid Hydrogen (GODU-LH2) utilized Integrated Refrigeration and Storage (IRAS) technology to condition LH_2 anywhere along the saturation curve, from the triple point to the maximum allowable working pressure of the storage tank, and opened up unique capabilities such as zero-loss storage and transfer, in-situ liquefaction, and densification of the stored fluid [1].

Central to the IRAS architecture is the coupling of a storage tank with a cryogenic refrigerator via an internal heat exchanger distributed throughout the fluid volume. This provides control over the bulk fluid properties inside the tank via direct addition and removal of thermal energy (heat), as opposed to the more traditional method of operational venting/pressurizing, followed by liquid replenishment. In the case of GODU-LH2 a 125,000 liter horizontal-cylindrical LH_2 storage tank was retrofitted with a custom tubular flow-through heat exchanger, and mated to a Linde Cryogenics LR1620 helium refrigerator capable of producing 390 W or 850 W of cooling at 20 K with and without liquid nitrogen (LN_2) precooling respectively. This refrigeration capacity provided a lift-to-tank heat leak ratio between 1.5 and 2.7, which was enough positive margin to densify the LH_2 to the triple point and create an appreciable amount of solid hydrogen [2].

In addition to the lift-to-heat leak ratio, many factors play a role in the ultimate performance of an IRAS system. Primary among them are the design of the internal heat exchanger—which is itself a function of many varying factors such as fluid species, tank geometry, and ease of fabrication—and the

overall hardware integration scheme, both of which have been reported on previously for GODU-LH2 [3,4]. Such a large landscape of variables complicates efforts to accurately predict the final performance of a desired IRAS system up front; and in many cases, only a few high level requirements can be sufficiently established at the outset of the design. Many thermo-fluid software packages exist that are capable of modeling virtually any scale IRAS system, however, validating the results is difficult due to the lack of experimental test data. Furthermore, obtaining these data can present a challenge for anyone pursuing a new design due to the relative difficulty of building even a simplified working test rig, and this is especially true for large scale systems where the cost of constructing a test setup can be difficult to justify to funding managers or investors.

It was a fundamental goal of the GODU-LH2 project to address this issue by gathering invaluable hydrogen temperature and pressure data at numerous fill levels, and over various system operational paradigms. Following the test campaign these data were used to anchor physics models built to predict various aspects of the system behavior. Of particular interest was the transient response during densification testing. These models will be the central topic of this paper.

2. GODU-LH2 IRAS Tank Instrumentation

Details regarding the design and construction of the entire GODU-LH2 system have been reported previously [3,4], therefore, only the inner IRAS tank instrumentation details will be presented in order to better understand the data used to anchor the analysis. Figure 1 shows the three temperature rakes used to map the hydrogen temperature profile, along with the relative position of the four fill levels tested; and table 1 reports the coordinates (corresponding to figure 1) of each sensor. Sensors were silicon diode type with accuracies of ±0.5 K from 450 K to 25 K, and ±0.1 K from 25 K to 1.5 K. Pressure data was collected by 0-689 kPa(abs) transducers that communicated with the ullage space through tubes that interfaced to the primary tank vent. Each unit had an error of ± 6.89 kPa.

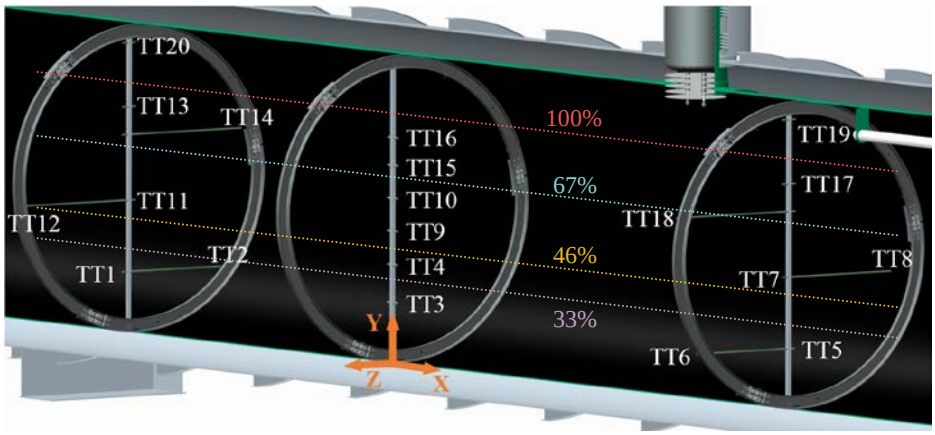

Figure 1. GODU-LH2 IRAS Tank Temperature Rakes & Relative Positions of Test Fill Levels

Table 1. Temperature Sensor Coordinates inside the IRAS Test Tank

	Distance, m				Distance, m		
Sensor #	X-dir	Y-dir	Z-dir	Sensor #	X-dir	Y-dir	Z-dir
TT1	-4.11	0.57	0.16	TT11	-4.11	1.24	0.00
TT2	-4.11	0.57	-0.99	TT12	-4.11	1.24	1.27
TT3	0.12	0.57	0.08	TT13	-4.11	2.12	0.00
TT4	0.12	0.92	0.08	TT14	-4.11	1.85	-1.22
TT5	6.27	0.57	0.00	TT15	0.12	1.85	0.08
TT6	6.27	0.57	1.15	TT16	0.12	2.12	0.08
TT7	6.27	1.24	0.16	TT17	6.27	2.12	0.00
TT8	6.27	1.24	-1.10	TT18	6.27	1.85	1.39
TT9	0.12	1.24	0.08	TT19	6.27	2.72	0.00
TT10	0.12	1.54	0.08	TT20	-4.11	2.72	0.00

3. Transient Data Set

Predicting the hydrogen pressure and temperature trends of the GODU-LH2 system during densification testing was the primary focus of the transient analysis. During densification the refrigeration system was operated at maximum capacity with the IRAS tank closed (i.e. no mass in or out). Because the lift-to-heat leak ratio was well over unity, the LH_2 gradually began to cool below the normal boiling point of 20.3 K (for para-hydrogen), and followed the saturation curve down toward the triple point of 13.8 K. Pressure also followed suit due to the closed tank, decreasing in lock-step with the temperature.

These tests were carried out at three different LH_2 fill levels—46% (57,500 L), 67% (83,750 L) and 100% (125,000 L)—and exhibited similar and expected behavior, with time scales increasing with the increase in hydrogen mass. Figure 2 shows the consolidated densification data for each fill level. Different tests are delineated by vertical lines and individually labeled for clarity, and temperature sensor call-outs (e.g. TT1, TT2, etc.) correspond to figure and table 1. The x-axis is in units of hours, however, because the tests were not carried out in sequence it is purposely not labeled. A 100 hour gauge is supplied to give a sense of temporal scale, and can be applied within an individual test series. Additionally, "analysis regions" are shown within each test series that establish the time slices corresponding to the analyses presented in the following sections.

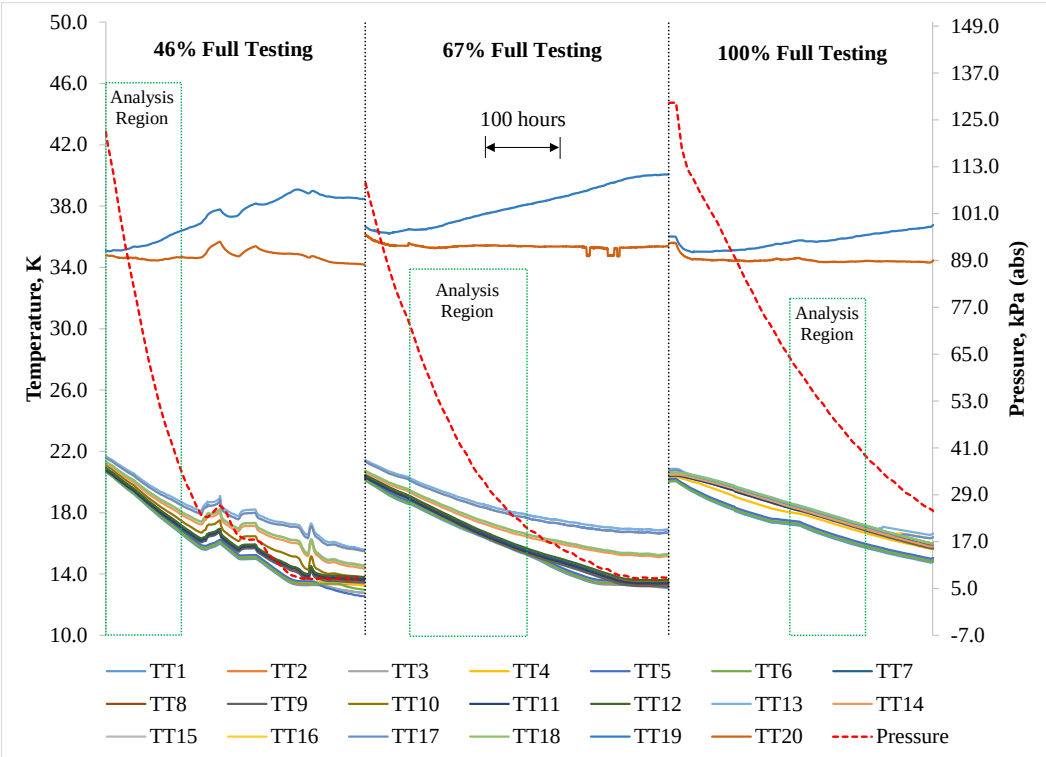

Figure 2. GODU-LH2 Densification Test Data At 46%, 67%, & 100% Fill Levels

3.1. Choice of transient analysis regions

Developing predictive models that could capture every conceivable system perturbation would be exceedingly difficult. Instead, the analytical models assumed consistent, but not necessarily constant, parameters over time. This approach demanded that time slices from the three densification tests be chosen during periods when the system was operating consistently, and without interruption. Also, the duration of time had to be long enough to sufficiently capture the system behavior. At the 46% and 100% fill levels the analysis envelope was 100 hours in duration, and 150 hours long at 67% full; these correspond to the regions called out in figure 2. Within these envelops the depressurization and temperature decrease was relatively smooth and consistent, fulfilling the requirement for stable system operation needed to match the physics models.

4. Transient Models

A thorough description of the workings of each analysis would be much too cumbersome and excessive to be presented here; therefore only high-level details and results will be discussed. However, step-by-step details of each, as well as a more complete examination of the results can be found in reference 5.

Two different transient models were constructed in an attempt to fully understand the GODU-LH2 system behavior over all three fill levels examined. The primary difference between them was the assumption pertaining to the condition of the stored liquid: fully saturated, versus subcooled with a saturated liquid layer separating the bulk liquid and vapor. As the simpler of the two, the former was the first to be developed and showed great promise at the lower fill level. However, as the level increased its accuracy waned, leading to the development of the latter.

Each model was constructed in Microsoft Excel, coded in Visual Basic, and utilized the Reference Fluid Thermodynamic and Transport Properties Database (RefProp, version 8) imbedded fluid properties solver to obtain the hydrogen and helium (GHe) properties as functions of different parameters. Spreadsheets were setup with user-defined initial and boundary conditions such as total tank volume and fill level, tank pressure, and hydrogen temperature(s). These values were then fed into a separate part of the spreadsheet that calculated new quantities based on the particular model methodology. The Visual Basic code handled iterative duties such as time accumulation and converging certain fluid properties for a given time step, and then tabulated the properties of interest for comparison to test data. Models were rendered insensitive to tank size/geometry or stored cryogenic fluid species by assuming uniform heat exchange and mixing within different fluid regions.

Mechanically, models were lumped node type schemes, forward-stepping in time. In general, liquid and vapor regions were defined as different nodes, and then the lift-to-heat leak ratio was used to determine how the hydrogen pressure and temperature were affected over time. Migration of mass from the ullage into the liquid via condensation as a result of the excess refrigerator lift was also taken into account. Both constant and variable helium refrigerant inlet conditions (temperature, pressure and mass flow rate) were explored—variable versions were obtained from curve-fit functions of refrigerator performance data gathered during testing, and constant quantities were averages over the same time.

Common between the two models were the assumptions that all refrigeration lift occurred in the liquid region (driven by the particular design and refrigerant flow path of the GODU-LH2 heat exchanger), and that the temperature of the helium exiting the heat exchanger was equal to that of the liquid (i.e. the heat exchanger was 100% efficient). Models both ran with 15 minute time increments, and each new iteration began by updating the helium inlet temperature, pressure and mass flow rate per the refrigerator data curve fits (in the case of the variable inlet conditions), and also took into account the heat absorbed in the vacuum-jacketed supply line connecting the refrigerator to the IRAS tank (determined by prior analysis and assumed constant). By prescribing the heat exchanger outlet temperature to the LH_2 temperature calculated in the preceding iteration, a new gross heat lift could be determined using the updated inlet values; and a net heat lift for the iteration was determined by accounting for the total tank heat leak (determined by boiloff calorimetry testing on the IRAS tank, and assumed constant at a given fill level).

Figure 3 depicts the analytical setup of both models with relevant variables called-out. The two are very similar, with the most obvious difference being the addition of a saturated liquid layer separating the saturated vapor and subcooled liquid regions in the subcooled model setup—this detail will be discussed later. Common to both are the environmental heat leak into the vacuum-jacketed GHe supply line ($\dot{Q}_{VJ,supply}$) and through the tank into the liquid and vapor regions ($\dot{Q}_{HL,liq}$ & $\dot{Q}_{HL,vap}$); the heat extraction taking place in the heat exchanger ($\dot{Q}_{Lift}$), as well as the inlet GHe temperature and pressure (T_{in} & P_{in}) and exit temperature (T_{out}); the GHe temperature, pressure and mass flow rate supplied from the refrigerator ($T_{GHe,supply}$, $P_{GHe,supply}$, & $\dot{m}_{GHe,supply}$); and finally, the mass flow rate of the condensed vapor into the liquid ($\dot{m}_{condense}$). In addition, the subcooled model includes the upper and lower temperature, and heat transfer across the saturated liquid layer (T_{vap}, T_{liq}, & $\dot{Q}_{SL}$); and its thickness (L_{SL}).

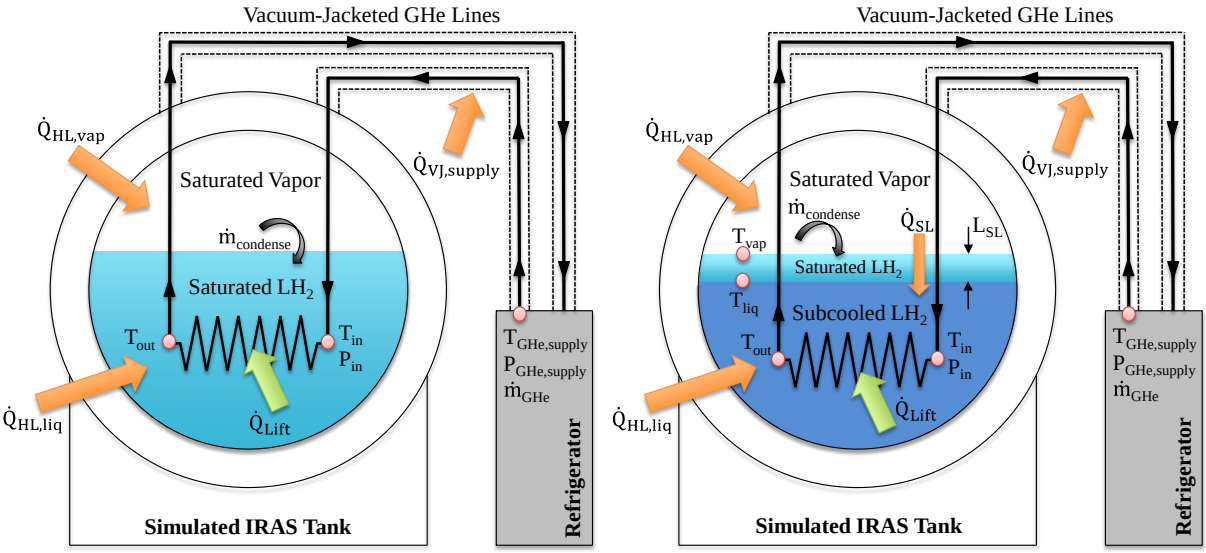

Figure 3. Analytical Setup for the Saturated Model (left), and Subcooled Model (right)

4.1. Saturated Model

The first of the two models developed was predicated on the core assumption that the entire tank existed at the saturation condition during densification testing. A completely saturated tank meant that the hydrogen properties could be defined by just one parameter (the tank pressure in this case), and both the temperature and pressure of the liquid and vapor would be equal, which provided a convenient parameter for convergence within the analysis. Within each time iteration the liquid density increase caused by $\dot{Q}_{Lift}$ was reflected in the vapor-to-liquid mass ratio. This ratio was adjusted by the code until the liquid and vapor pressures converged, and then the analysis continued onto the next time iteration.

Figures 4 and 5 show the pressure and temperature results of the saturated model for each fill level, and for each helium inlet condition (i.e. variable versus constant properties). Temperature data is averaged across diodes 1 through 18, (see figure 1), and error bars shown in the plots are: pressure = ±6.89 kPa, and temperature = ±0.1 K.

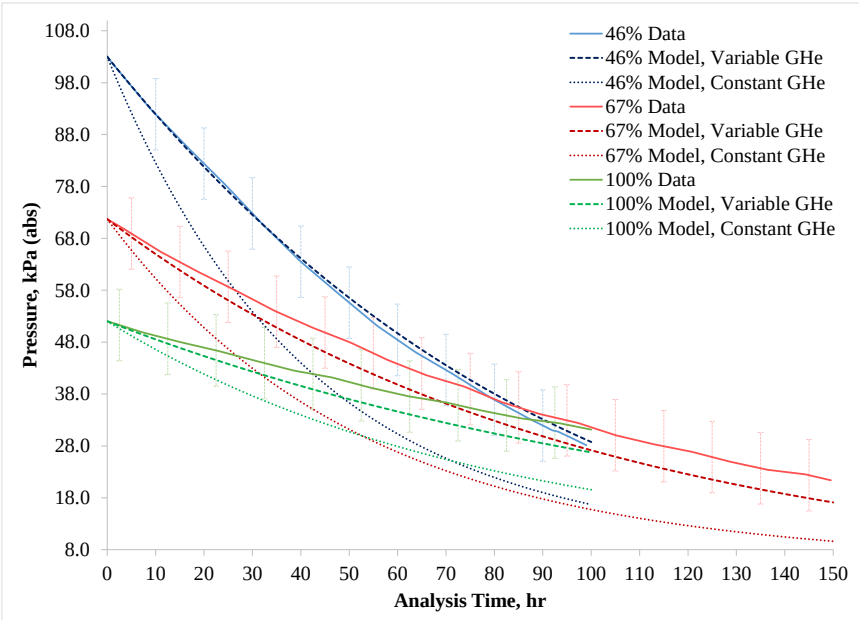

Figure 4. Saturated Model Depressurization Prediction vs. Experimental Data for Each Fill Level

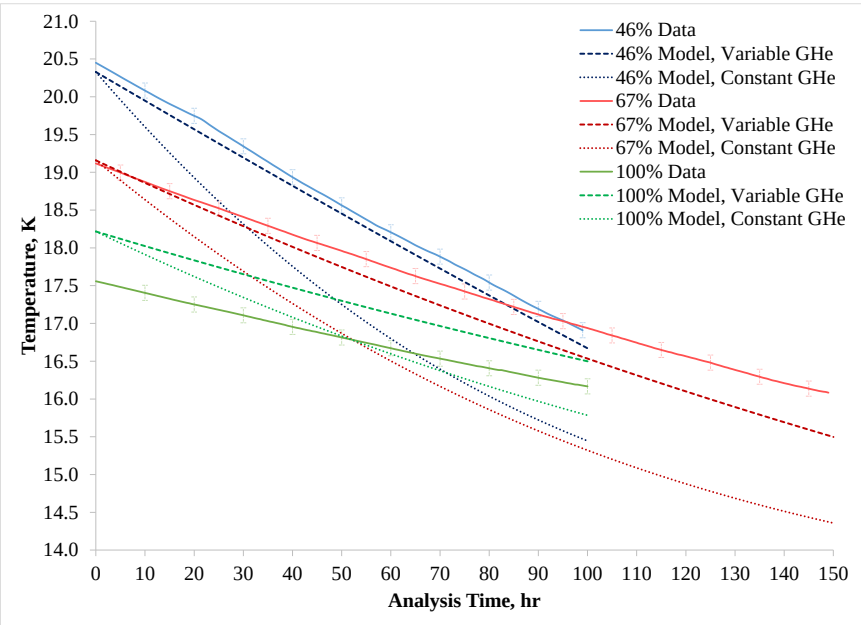

Figure 5. Saturated Model Temperature Prediction vs. Experimental Data for Each Fill Level

4.1.1 Discussion of Saturated Model Results. Figures 4 and 5 reveal that assuming constant GHe inlet conditions leads to dramatically inaccurate predictions of the depressurization and temperature drop. In each case this simulation fell well outside the error envelopes, and were, at times, greater than 50% lower than the pressure test data, and 10% lower than the temperature data, which leads to the conclusion that such a simplification is probably not reasonable for modeling IRAS systems. Instead, some knowledge of how the refrigerator outlet conditions vary must be possessed or obtained prior to conducting an analysis.

Conversely, variable GHe properties cases predicted both the temperature and pressure trends with striking accuracy at the 46% fill level. Although the pressure predications fell within the error bounds at each fill level for the chosen time slices, at 46% full the model appeared to almost perfectly mimic the test data. This was also the case for the temperature prediction, although it failed to fall within the error bounds; nevertheless, the model trended extremely close to the data, and was consistent over the entire duration. This seems to substantiate the assumption that the entire tank was saturated. However, examination of the other two fill levels reveals contrary behavior. Depressurization predictions at both the 67% and 100% fill levels seemed to diverge from the data as time increased, and although the temperature at 67% appears to have indeed been saturated at the outset of the simulation, it also diverges. At the 100% level the initial simulation temperature (i.e. the saturation temperature at the initial pressure) was well above the actual tank temperature. This effectively proves that the tank was not fully saturated at the 100% fill level, and because all of the 18 diodes were submerged at that level, the temperature curve presented in figure 5 is the average value of the liquid itself. It was therefore reasoned that the bulk liquid must be subcooled; and in addition, the fact that the model over-predicted the depressurization rate suggested that the heat transfer between the liquid and ullage must have been suppressed. These two interpretations lead to the updated analysis scheme presented next.

4.2. Subcooled Model

Following the failure of the saturated model to accurately predict the transient behavior at 100% full a separate model was developed that abandoned the totally saturated assumption in favor of a more complicated scheme using subcooled liquid. This subcooled model was predicated on three primary assumptions: (1) the vapor was saturated at the tank pressure—and by extension, so was the liquid-to-vapor interface; (2) refrigeration lift caused subcooling of the liquid; and (3) a layer of saturated liquid

separated the ullage from the subcooled liquid. It was thought that this saturated liquid layer would suppress the heat transfer between the liquid and vapor, and increase depressurization times. Giving credence to this assumption was the fact that the heat exchanger was essentially completely submerged at the 100% fill level, conceivably allowing for a uniform layer to exist over virtually the entire liquid-to-vapor surface area. This approach was similar to a model used by Ewart and Dergance in 1978 [6], only the liquid layer was assumed to be stratified instead of completely saturated, and wall boundary layers were taken into account that fed the stratified layer with less dense fluid.

Mechanically, both models were similar. However, where the saturated model converged on the solution that equated the liquid and vapor pressures before moving onto the next time step, the subcooled model calculated the pressure as a function of the heat removed from the vapor. This heat removal was determined by balancing the mass and energy into and out of the vapor, liquid, and saturated layer regions. The sub-boiling point bulk liquid established a ΔT across the saturated liquid layer (i.e. T_{vap}-T_{liq}), and associated heat transfer through it ($\dot{Q}_{SL}$). This heat transfer was assumed to be via pure conduction through the layer—governed by the thermal conductivity of the saturated liquid, liquid-to-vapor surface area (A_{LV}) , and L_{SL}—and via the heat of vaporization at the liquid-to-vapor interface.

L_{SL} was a critical variable in the analysis, as it dramatically affected the thermal resistance between the subcooled liquid and vapor. To estimate this thickness, steady state data was used from prior GODU-LH2 zero boil-off pressure control (ZBO-PC) testing [7] at the 100% fill level. It was presumed that during steady state operation the heat transfer rate through the saturated layer must be equal to that leaking into the ullage in order to maintain constant pressure (i.e. $\dot{Q}_{SL} = \dot{Q}_{HL,vap}$). Using the average vapor and subcooled liquid temperatures during ZBO-PC testing, A_{LV} (determined via geometric relations), and the known $\dot{Q}_{HL,vap}$, it was possible to back out an estimate for L_{SL} using Fourier's equation. L_{SL} was found to be roughly 35 mm at the 100% fill level, and was assumed constant throughout the subcooled analysis. Figure 6 compares the pressure and temperature results of the subcooled and saturated simulations using variable GHe properties at 100% full.

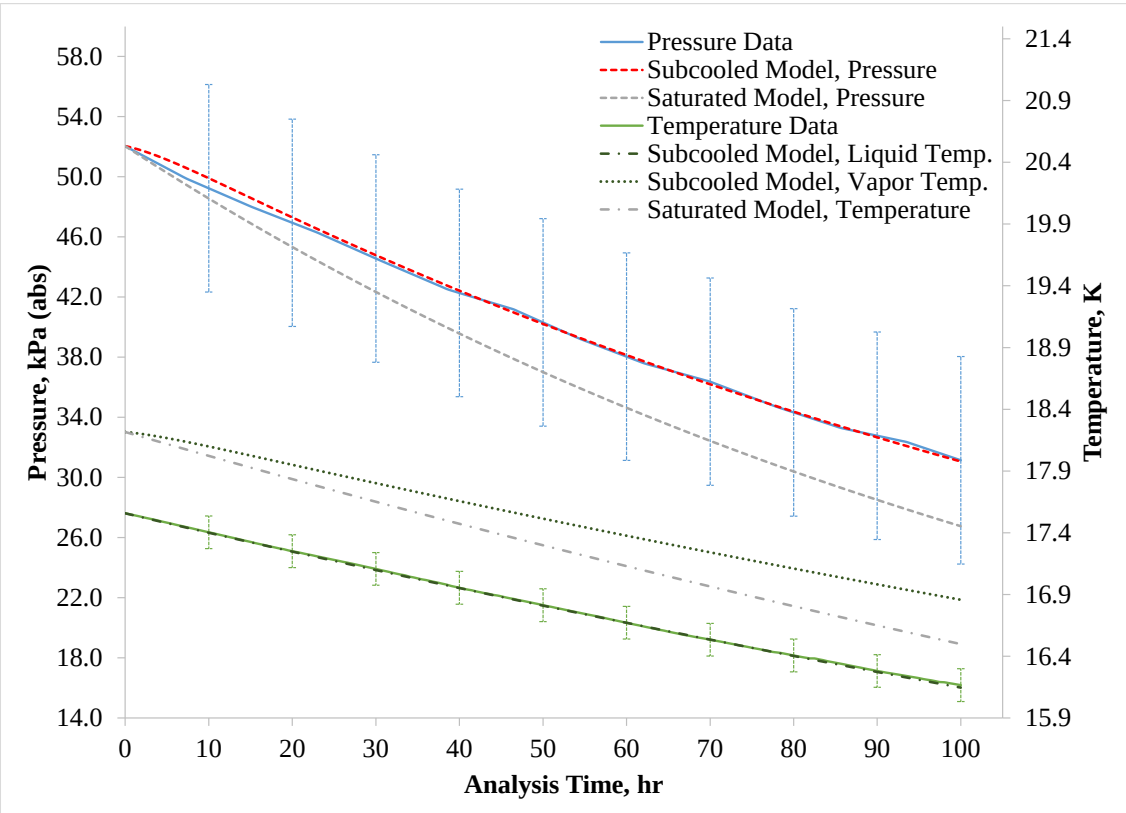

Figure 6. Subcooled Model Results at 100% Fill Level

4.2.1 Discussion of Subcooled Model Results. Figure 6 shows that the subcooled model predicted both the depressurization and temperature trends at 100% full much more accurately than the saturated model—save the slight delay of the pressure curve to react at the beginning of the simulation, which was due to the sensitivity of the saturated liquid layer thickness on the thermal resistance. The difference between data and prediction for the pressure was -0.06 kPa on average, with a standard deviation of 0.12. This result was a marked improvement over the saturated model, where the slope of the variable GHe case was greater than that of the data by anywhere from 7% to 14% over the last quarter of the simulation, and the difference between the data and the prediction was -4.2 kPa on average, with a standard deviation of 0.23. Prediction of the liquid temperature was virtually exact, with an average absolute error of 0.03% over the entire 100 hour simulation time, with a maximum of 0.12%.

Omitted from figure 6 for sake of clarity, the constant GHe properties simulation did not result in the drastically different behavior observed in the saturated model. It did however, appear to exhibit divergent behavior toward the end of the simulation time, whereas the variable case seemed to maintain a similar slope to the data curve. The subcooled model was also applied to the 67% fill level, as it exhibited some traits that can be attributed to a non-fully saturated tank. Compared to the saturated results, slopes of the pressure and temperature curves showed closer agreement to the data over the entire 150 hour time slice, and did not seem to exhibit any divergent behavior—however, accuracy was still lower than at 46% full for the saturated model, and 100% full for the subcooled simulation.

5. Conclusion

Two different simulation schemes were developed to predict the transient behavior of large scale Integrated Refrigeration and Storage (IRAS) systems. With future applicability in mind, these models were built to be as general as possible—agnostic with respect to stored fluid species, tank size and geometry. Experimental test data gathered during a liquid hydrogen IRAS test campaign at NASA KSC were used to anchor the analyses, and pressure and temperature trends showed close agreement with data depending on fill level and simulation.

6. References

[1] Notardonato, W., Swanger, A., Fesmire, J., Jumper, K., Johnson, W. and Tomsik, T. (2017), Final test results for the ground operations demonstration unit for liquid hydrogen. Cryogenics, 88, pp.147-155.

[2] Swanger, A. M., Notardonato, W. U., Fesmire, J. E., Jumper, K. M., Johnson, W. L. and Tomsik, T. M. (2017), Large scale production of densified hydrogen to the triple point and below, Advances in Cryogenic Engineering, IOP Conf. Series: Materials Science and Engineering 101, doi:10.1088/1757-899X/278/1/012013

[3] Fesmire, J. E., Tomsik, T. M., Bonner, T., Oliveira, J. M., Conyers, H. J., Johnson, W. L. and Notardonato, W. U. (2014), Integrated heat exchanger design for a cryogenic storage tank, Advances in Cryogenic Engineering, AIP Conference. Proceedings, Vol. 1573, pp.1365-1372, doi:10.1063/1.4860865

[4] Swanger, A. M., Notardonato, W U., Johnson, W. L. and Tomsik, T. M. (2016), Integrated Refrigeration and Storage for Advanced Liquid Hydrogen Operations., Cryocoolers 19, 19th International Cryocooler Conference Proceedings, Vol.19, pp.513-522

[5] Swanger, A., (2018), Large Scale Cryogenic Storage with Active Refrigeration, M.S. thesis, University of Central Florida, USA, http://stars.library.ucf.edu/etd/

[6] Ewart, R. O. and Dergance, R. H., (1978), Cryogenic Propellant Densification Study, NASA CR-159438

[7] Notardonato, W. U., Swanger, A. M., Fesmire, J. E., Jumper, K. M., Johnson, W. L. and Tomsik, T. M. (2017), Zero boiloff methods for large scale liquid hydrogen tanks using integrated refrigeration and storage, Advances in Cryogenic Engineering, IOP Conf. Series: Materials Science and Engineering 101, doi:10.1088/1757-899X/278/1/012012